The effect of Fe$_{Ga}$ (0/–) level presence on material properties in dilute Al$_x$Ga$_{1-x}$N layers

L. Sun,[1,a] [ID] P. Kruszewski,[2] [ID] V. P. Markevich,[1] [ID] C. A. Dawe,[1] [ID] A. R. Peaker,[1] [ID] I. F. Crowe,[1] [ID] J. Plesiewicz,[2] [ID]
P. Prystawko,[2] [ID] Sz. Grzanka,[2] [ID] E. Grzanka,[2] [ID] R. Jakiela,[3] D. Binks,[1] [ID] and M. P. Halsall[1] [ID]

AFFILIATIONS

[1]Photon Science Institute and Department of Electrical and Electronic Engineering, The University of Manchester,
Manchester M13 9PL, United Kingdom
[2]Institute of High Pressure Physics, Polish Academy of Sciences, Warsaw 01-142, Poland
[3]Institute of Physics, Polish Academy of Sciences, al. Lotników 32/46, Warsaw 02-668, Poland

Note: This paper is part of the special topic, Defects in Semiconductors 2024.
[a]Author to whom correspondence should be addressed: ijie.sun-3@postgrad.manchester.ac.uk

ABSTRACT

Al$_x$Ga$_{1-x}$N epilayers are used as the basis of ultraviolet LEDs and detectors. The trap states produced by defects and impurities can play a key role in the device performance. In this work, conventional deep-level transient spectroscopy, photoluminescence (PL), and secondary ion mass spectrometry have been used to characterize a deep-level trap termed as E3 in dilute Al$_x$Ga$_{1-x}$N (x < 0.063) epilayers grown by metal-organic vapor phase epitaxy (MOVPE) on highly conductive ammono-GaN substrates. The Al$_x$Ga$_{1-x}$N epilayers were doped with silicon to about 3×10^{16} cm^{-3}. The electrical and the optical measurements were conducted on Ni/Au Schottky barrier diodes and virgin samples, respectively. First, we observed a general trend that the E3 (Fe$_{Ga}$) electron trap concentration significantly changes along the wafers in Al$_x$Ga$_{1-x}$N layers that is fully consistent with previously reported results for GaN materials grown by the MOVPE technique. Second, we report that the activation energies for electron emission for the E1 and E3 traps in dilute Al$_x$Ga$_{1-x}$N exhibit linear variations with Al content. Moreover, low-temperature PL results show a proportional relation between the intensity of the line with its maximum at 1.299 eV and concentration of residual Fe impurity. Finally, we discuss how the presence of defects resulting from Fe contamination may result in degradation of Al$_x$Ga$_{1-x}$N-based devices.

I. INTRODUCTION

After decades of development, GaN and its alloys have emerged as important wide-bandgap semiconductor materials and have found widespread technological applications.[1–3] In addition to achieving n-type and p-type doping of the materials for the formation of junctions, the bandgap engineering from infrared (InN) to ultraviolet (AlN) is possible by altering the alloy composition.[3] Benefiting from the outstanding physical properties of GaN-based semiconductor materials, allowing the production of HEMT transistors,[4] power devices as well as highly efficient light emitting diode (LEDs) and laser diode (LDs).[1,3,5,6] However, the development of GaN-based materials has relied on advances in the understanding of native defects, unintentional contaminants as well as

dopant impurities.[3,7] Both impurity-related defects and native lattice defects, which act as carrier traps or recombination centers within the bandgap, can play a pivotal role in influencing the performance and reliability of GaN/Al$_x$Ga$_{1-x}$N devices. These defect-related effects are well known, such as compensation by native point defects which decreases the level of doping and carrier lifetime degradation by deep-level defects which can act as recombination centers, hindering the efficiency light emission from LEDs. Therefore, identifying and controlling such defects in actual devices is essential.[2,7]

There have been many studies devoted to discovering impurity-related defects in GaN-based materials. It has been reported that some impurities are introduced through epitaxial growth and originate from precursors and carrier gases, such as carbon, oxygen,

and hydrogen.[1,8,9] These impurities can be found in most GaN-based materials.[1,7] The incorporation of such impurities into the material can be mitigated during epitaxial growth through specific technical measures, thereby reducing their impact on the material properties.[7,9–11] Unfortunately, the sources of some impurities or defects, such as iron (Fe), remain ambiguous. In 2002, Heikman et al.[9] used ferrocene as a Fe dopant for metal-organic chemical vapor deposition (MOCVD) growth of semi-insulating GaN and explained that the introduction of Fe was insensitive to growth conditions but suffered from memory effects, such as adsorption/desorption from reactor walls and plumbing, rather than from reactor environment related effects.[10] Therefore, in this regard, Fe is similar to magnesium (Mg) doping of GaN by MOCVD.[9] However, other studies suggest that the Fe impurities may originate from the wafer cleaning process[1] or via Fe diffusion from reactor components.[12] In general, the iron impurity source is not related to the carrier gases or metalorganics, as Fe content in the layers weakly depends on molar flows of reagents. Most likely, it originates from the reactor components, probably the susceptor coating as argued by Horita et al.[12] and by Zhang et al.[1] They noted that the size of the substrates, because this determines the coverage of the susceptor, significantly influences the Fe incorporation in the GaN epilayer. It was argued that the CVD coating of the graphite susceptor contains some iron which tends to evaporate at elevated growth temperatures.[1] Assuming this impurity is emitted at a constant rate, it diffuses over the surface from the edge of substrate toward the wafer center and is not introduced by mass transport from the gas phase. This effect can be reduced by using large GaN wafers (single wafer reactor geometry) and additional treatment of the susceptor (purer coatings, pre-conditioning with deposition of a stable barrier coating like AlN, etc.). In addition, due to the constant rate of emission of this impurity, it can be further reduced by increasing the growth rate of the layers. Fe has been reported to act as a compensating deep acceptor-like point defect in semi-insulating GaN films grown on sapphire by metal-organic vapor phase epitaxy (MOVPE),[9,10,13] which has the potential to significantly disrupt the density of the two-dimensional electron gas (2DEG) within the channel of GaN/AlGaN high-electron-mobility transistor (HEMT) structures.[14] Since Fe-related defects could compensate donors, the on-state resistance in GaN-based devices may increase, and a substantial delay in the switching operation can be induced, resulting in an emission time constant of several tens of milliseconds at room temperature.[12]

In order to investigate deep-level defects in GaN-based materials, researchers have used junction spectroscopy techniques such as deep-level transient spectroscopy (DLTS) and also high-resolution Laplace DLTS (L-DLTS) to measure the energy level positions and accurately determine the thermal ionization energies (E_A) of defects. An energy level at round Ec–0.58 eV, where Ec is the conduction band minimum, which is usually referred to as the E3 electron trap, has been assigned to a Fe_{Ga} acceptor level.[12,15–17] Horita et al.[12] have convincingly reported that the E3 traps concentration is strongly correlated to the Fe concentration in GaN grown by MOVPE and argued that the E3 trap originates from Fe on Ga sites. We recently reported results regarding the E3 trap which are consistent with

those in the literature and support its recent identification as an acceptor level of Fe_{Ga}.[16–18]

From previous PL measurements studies, it can be concluded that Fe trace impurities within gallium nitride (GaN) epitaxial layers are responsible for an infrared PL band, primarily characterized by a sharp zero-phonon line (ZPL) at around 1.299 eV, which is caused by the Fe_{Ga}^{3+} charge state via the $^4T_1(G) \rightarrow {}^6A_1(S)$ spin-forbidden transition.[15,19–25] Although, it appears that the intensity of Fe^{3+}-related luminescence is not dependent on the Fe concentration from previous literature results,[23] we show here that the relative PL intensity remains positively correlated with iron concentration. Thus, based on our experimental observations, we propose using PL as a characterization method to assess the Fe in GaN layers with low Fe concentrations ($\leq 10^{17}$ cm^{-3}).

In this work, we also report that the activation energies of electron emission for the E1 and the E3 traps exhibit similar linear variations with Al content in the dilute $Al_xGa_{1-x}N$ (x $\leq$ 0.063) system. We find that the concentration of the E3 electron trap strongly depends on the position from the edge to the center for all $Al_xGa_{1-x}N$ samples discussed in this paper. We show that, as in pure GaN, the concentration of the E3 trap is strongly correlated with iron concentration determined by SIMS in our representative sample of $Al_{0.05}Ga_{0.95}N$. The results were obtained by employing DLTS, PL, and SIMS and are consistent with the results of Horita et al. for GaN.[12] Additionally, we infer that the presence of the defects caused by higher Fe concentrations may result in the degradation of device characteristics.

II. EXPERIMENTAL DETAILS

Figure 1 shows the sample structure diagrams of one reference GaN and three dilute $Al_xGa_{1-x}N$ (x $\leq$ 0.063) layers grown by MOVPE on 1-in. highly conductive (n $\sim 1 \times 10^{19}$ cm^{-3}) ammono-GaN substrates at the Institute of High Pressure Physics

Samples structure

1.7 µm Al$_x$Ga$_{1-x}$N:Si (3E16 cm-3)

100 nm GaN:Si (5E17 cm-3)

400 nm GaN:Si (2E18 cm-3)

Ammono-GaN (n-GaN)

where, x = 0, 0.025, 0.05 and 0.063

FIG. 1. Sample structure diagram of the dilute Al$_x$Ga$_{1-x}$N (x $\leq$ 0.063) layers grown by metal-organic vapor phase epitaxy (MOVPE) on highly conductive n-type ammono-GaN substrates.
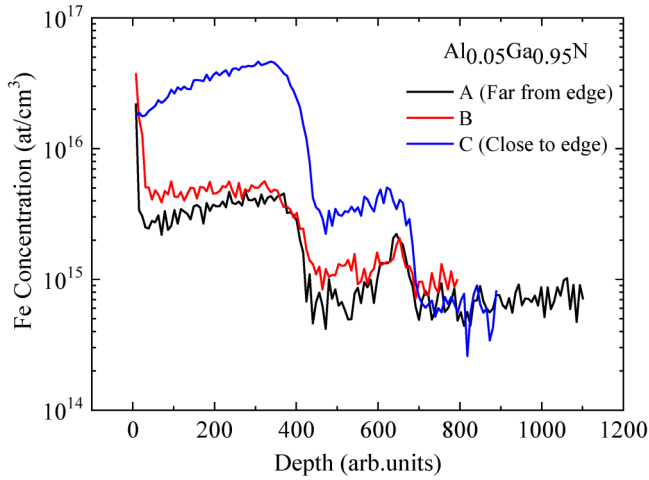
11 May 2024 05:34:50

FIG. 2. SIMS depth profiles of Fe concentration along the growth direction of the dilute $Al_xGa_{1-x}N$ sample (x = 0.05), comparing Fe concentration at different positions on the wafer from A (far from to the edge) to C (close to the edge).

FIG. 3. Current density–voltage (J–V) dependencies for the Schottky diodes on the dilute $Al_xGa_{1-x}N$ (x = 0.05) sample on different positions from the edge to the center, measured at 300 K.

of the Polish Academy of Sciences.[26,27] As shown in Fig. 1, the 3×10^{16} cm^{-3} Si-doped 1.7 μm thick $Al_xGa_{1-x}N$ top layer was grown on highly conductive GaN:Si layers. XRD (x-ray diffraction) data confirmed that dilute $Al_xGa_{1-x}N$ layers are fully strained to the lattice of the underlying GaN material. The (Ga + Al)/Si ratio was kept fixed at 12.8×10^6, and the pressure, temperature, and V/III ratio of the $Al_xGa_{1-x}N$ layers were 200 Torr, 1030 °C, and 3400, respectively.[18] In order to investigate the electrical properties of defects in dilute $Al_xGa_{1-x}N$ samples, we fabricated Ni/Au Schottky barrier diodes (SBDs) mounted on ceramic substrates and then connected to the Ti/Al/Ni/Au Ohmic contact with the use of silver paint. The Ni/Au Schottky contact on the top layers was connected to Au pads on the ceramic substrate using bonded gold wires.

Figure 2 shows SIMS depth profiles of Fe concentration along the growth direction of the $Al_{0.05}Ga_{0.95}N$ sample, comparing the Fe concentration at different positions on the wafer from A (far from the edge) to C (close to the edge). The SIMS results reveal a variation in Fe concentration with depth, ranging from approximately 10^{15}–10^{16} cm^{-3} in magnitude. Additionally, it is observed that the Fe concentration is much higher near the edge of the wafer, at the position (C), about 2×10^{16} cm^{-3} compared to the center of the wafer, at the position (A), around 2×10^{15} cm^{-3}. We suppose that the Fe source in our dilute $Al_xGa_{1-x}N$ samples most likely comes from the SiC-coated graphite susceptor used in the epitaxial growth in MOVPE system.

III. EXPERIMENTAL RESULTS

A. I–V measurements

Figure 3 shows current density–voltage (J–V) dependencies measured at 300 K for several SBDs on the $Al_{0.05}Ga_{0.95}N$ sample at different positions from the wafer edge to the wafer center under bias voltage from −5 to 2 V. The large apparent noise observed in
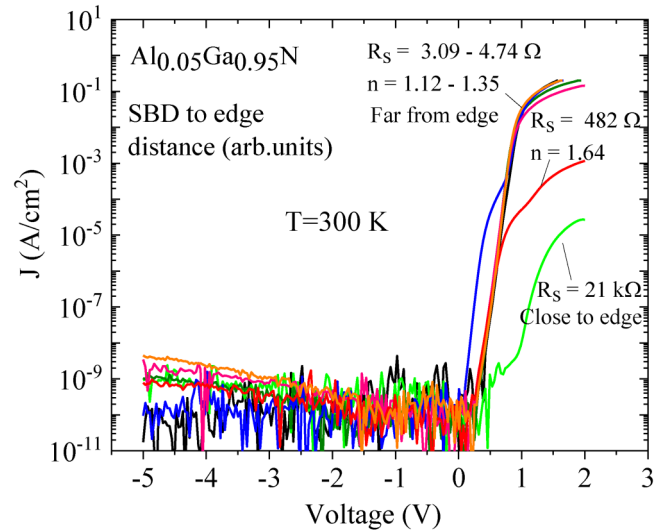
the reverse leakage current is due to the current approaching the measurement limit of the instrument. For the diodes near the wafer edge, the series resistance (R_s) is significantly higher than the diodes closer to the wafer center, with R_s values of 21 kΩ and 3 Ω, respectively. A similar trend for the measured ideality factor (n) is observed, as the position of the diode moves away from the wafer edge, n decreases from 1.64 down to 1.12.

B. Deep-level transient spectroscopy (DLTS)

Figure 4 shows conventional DLTS spectra recorded for different Al fractions of dilute $Al_xGa_{1-x}N$ samples (x = 0%, 2.5%, 5%, and 6.3%) and the relative measurement parameters used for recording of the spectra are given in the graph. The spectra are representative of electron capture/emission processes for deep-level trap levels in the regions from about 0.3 to 0.7 μm from the surface toward the substrate. The figure shows the two types of electron traps, commonly labeled as E1 and E3 observed using the DLTS rate window of 50 s^{-1}. As for the electron-emission-related peaks of GaN (x = 0%) samples, the maxima of the E1 and the E3 are at about 148 and 314 K, respectively, which are quite similar to the temperatures of the peaks reported in the previous literature for epi-GaN layers grown on free-standing GaN substrates.[12,28,29] The values of the DLTS signal on Y axis represents the $2 \times (\Delta C/C_b) \times N_d \times f$ values normalized by the maximum value of the E3 to better observe the temperature shift of the E3 level with varying Al composition changing from 0% to 6.3%. Note that ΔC is the amplitude of the capacitance transient, C_b is the capacitance measured at the applied reverse bias, N_d is the concentration of uncompensated donors, and f is the correction factor, which takes into account the Debye tail at the depletion depths at the bias and pulse voltages.[30,31] Moreover, the $2 \times (\Delta C/C_b) \times N_d \times f$ values at

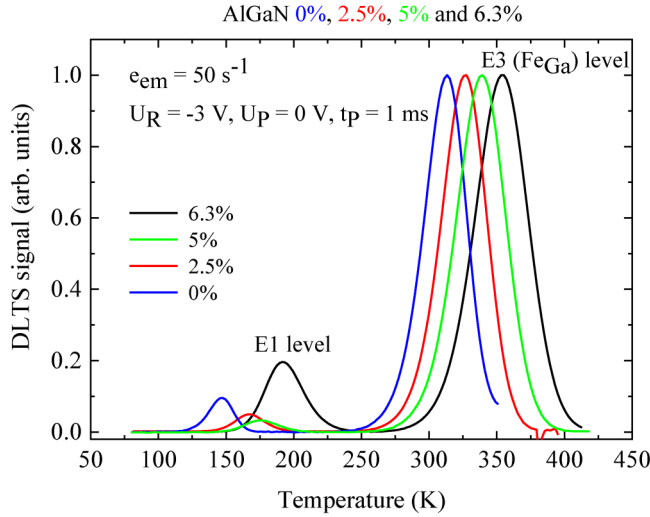**FIG. 4.** Conventional DLTS spectra normalized to the maximum value of the E3 (Fe$_{Ga}$) trap level intensity recorded for dilute Al$_x$Ga$_{1-x}$N samples with different Al contents (x = 0%, 2.5%, 5%, and 6.3%). The conventional DLTS was measured under a rate window (e$_{em}$) of 50 s^{-1}, with a fixed reverse bias voltage (U$_b$) of −3 V, a filling pulse voltage (U$_p$), and length (t$_p$) were kept as 0 V and 1 ms, respectively.

the peak maxima are close to the average trap concentrations (N$_T$) in the probed regions. It is evident from the graph that as the Al composition changes from 0, 0.025, 0.05, to 0.063, the E1 peak shifts from 148 to 168, 175, and 192 K, respectively. Meanwhile,

the E3 (Fe$_{Ga}$) peak shifts from 314 to 327, 339, and 354 K, respectively.

Figure 5(a) shows Arrhenius plots of the T^2 corrected electron-emission rates for the E1 and E3 Fe$_{Ga}$(0/−) trap levels for different Al content dilute Al$_x$Ga$_{1-x}$N samples (x = 0%, 2.5%, 5%, and 6.3%) measured with the use of DLTS, and the corresponding activation energy (E$_A$) values for E1 and E3 traps are given. As expected, the activation energy values for both trap E1 and trap E3 increase with increasing Al content in the Al$_x$Ga$_{1-x}$N. For the E1 trap, the activation energy values are 247, 286, 323, and 334 meV, corresponding to Al$_x$Ga$_{1-x}$N compositions of x = 0 (blue), 0.025 (red), 0.05 (green), and 0.063 (black), respectively. For the E3 trap, the activation energy values are 606, 644, 660, and 685 meV, corresponding to the same Al$_x$Ga$_{1-x}$N compositions. Upon extracting the activation energy values and their corresponding Al compositions of the E1 and E3 traps from Fig. 5(a) and subjecting them to linear fitting, Fig. 5(b) is obtained. Both data series have been fitted with a linear dependence and the fitting dependencies are $y = 1389 * x + 249$ and $y = 1169 * x + 608$ for the E1 and the E3 traps, respectively. Note that the units of the y axis here is meV.

Figure 6 shows the conventional DLTS spectra recorded for three Schottky diodes for a Al$_x$Ga$_{1-x}$N (x = 0.05) sample for different distances from the edge to the center of the wafer. The E1 and the E3 trap level peaks with their maxima at about 193 and 362 K for a DLTS rate window of 200 s^{-1} are observed in the recorded spectra. The value of the trap concentration plotted on the Y axis are derived using the formula, $2 \times (\Delta C / C_b) \times N_d \times f$ as mentioned above. However, in this case, the values are not normalized, which directly provides the average trap concentrations (N$_T$) in the probed regions. A large variation of the E3 Fe$_{Ga}$(0/−) trap concentration (N$_{T,E3}$) was observed from the edge to the center of the
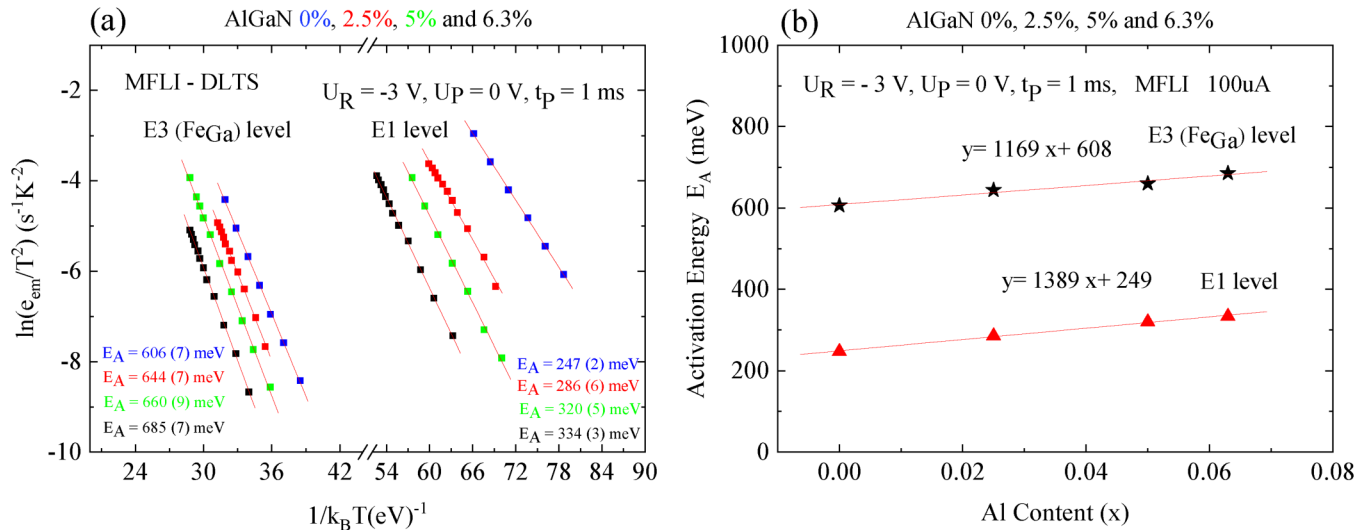

FIG. 5. (a) Arrhenius plots of T^2-corrected electron-emission rates for the E1 and E3 (Fe$_{Ga}$) trap levels for different Al contents for dilute Al$_x$Ga$_{1-x}$N samples (x = 0%, 2.5%, 5%, and 6.3%) measured with the use of DLTS and corresponding activation energies (E$_A$) determined from the linear fitting procedure. (b) The E$_A$ values extracted from (a) and the linear fitting plots of the E1 and theE3 (Fe$_{Ga}$) traps for increasing Al composition from 0% to 6.3%. The measurement parameters are given in the graph.
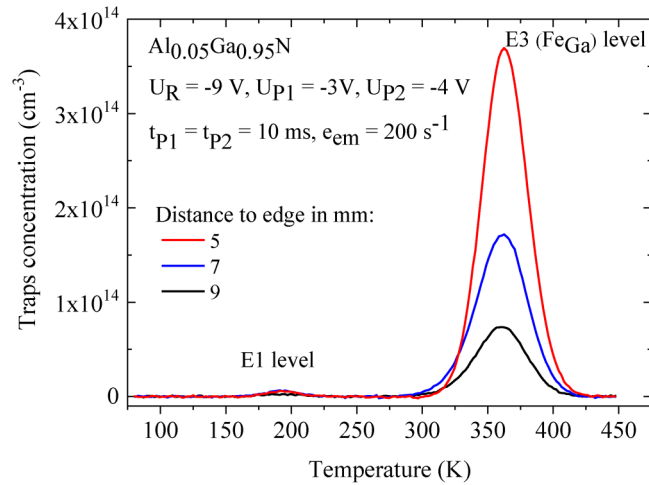
FIG. 6. Conventional DLTS spectra recorded for three Schottky diodes on the dilute $Al_xGa_{1-x}N$ (x = 0.05) sample at different distances from the edge to the center. Measurement parameters used for recording the spectra are given in the graph.

sample, however, the trap concentration of E1 is barely changed and most likely not directly related to Fe impurity or its complex.

C. Photoluminescence (PL)

Figure 7 shows the impact of the changing bandgap (E_g) of different samples of dilute AlGaN on the photoluminescence (PL)
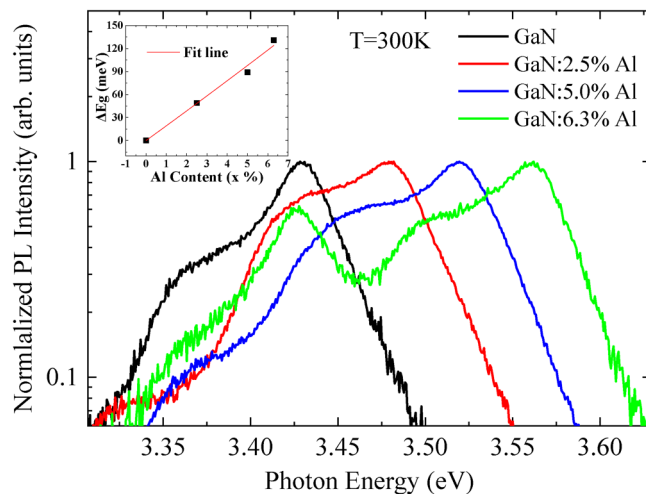

FIG. 7. Normalized photoluminescence intensity spectra for photon energies near band-to-band transitions in dilute $Al_xGa_{1-x}N$ samples (x = 0%, 2.5%, 5%, and 6.3%) measured at 300 K. The inset corresponds the fitting plots of the dilute $Al_xGa_{1-x}N$ bandgap shift in respect to GaN (x = 0%) for Al content x = 2.5% (ΔE_g = 49 meV), x = 5.0% (ΔE_g = 89 meV), and x = 6.3% (ΔE_g = 131 meV), respectively.

spectra measured at T = 300 K. The inset in Fig. 7 shows the plot of the dilute $Al_xGa_{1-x}N$ (x ≤ 0.063) bandgap shift vs Al fraction, and the fitting curve was calculated from the commonly known compositional dependence of the bandgap of $Al_xGa_{1-x}N$,[32]

$$E_g(x) = (1 - x)E_g(\text{GaN}) + xE_g(\text{AlN}) - bx(1 - x), \quad (1)$$

where b is the bowing parameter, and the room temperature energy bandgaps of GaN and AlN were taken as $E_g(\text{GaN}) = 3.43$ eV and $E_g(\text{AlN}) = 6.24$ eV, respectively. The bandgap shift in respect to GaN (x = 0%) is $\Delta E_g = 49$ meV for Al content x = 2.5%, $\Delta E_g = 89$ meV for Al content x = 5.0%, and $\Delta E_g = 131$ meV for Al content x = 6.3%. The bowing parameter was determined to be $b = 0.86 \pm 0.08$ eV, which is very close to commonly reported value of b = 1 eV.

Figure 8 shows low-temperature (10 K) PL intensity spectra recorded for three different positions from the edge to the center for the $Al_xGa_{1-x}N$ (x = 0.05) sample, which corresponds to the same positions used in the SIMS measurements from Fig. 2. The sample was held on the cold finger of the closed-cycle He optical cryostat and measured with CW excitation at 261 nm from a deep ultraviolet laser source all with the same low laser power of ~10 μW. Below, we discuss these PL conditions used in the experiment. Figure 8 presents the infrared emission band observed by PL with a dominant peak around 1.299 eV caused by the Fe_{Ga}^{3+} charge state via the $^4T_1(G) \rightarrow {}^6A_1(S)$ spin-forbidden transition, and also the sideband which is a superposition of a vibration replica of the main peak. It is evident that the PL intensity caused by the Fe_{Ga}^{3+} in sample A (near the edge) is significantly higher than that in sample C (near the center). This result is in agreement with DLTS and SIMS data confirming Fe variations across the wafer.
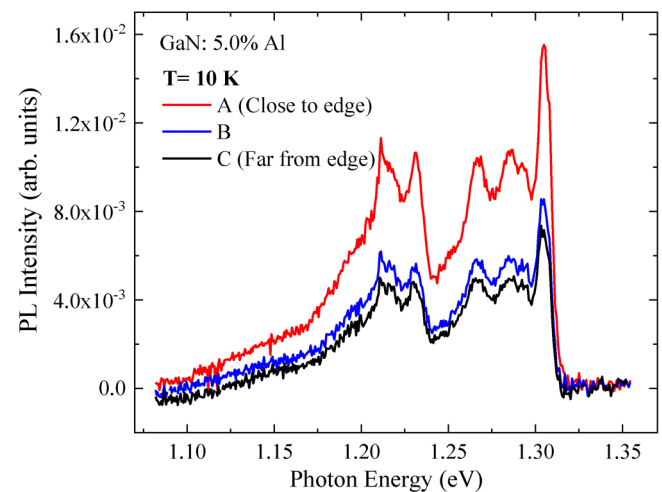

FIG. 8. Low-temperature PL intensity spectra recorded for three different positions from the edge to the center on the dilute $Al_xGa_{1-x}N$ (x = 0.05) sample.

IV. DISCUSSION

Our experimental results lead to three main observations.

(1) It is deduced from PL results that the dilute $Al_xGa_{1-x}N$ layers grown by MOVPE follow the compositional dependence of the energy bandgap of $Al_xGa_{1-x}N$ alloys. Moreover, the $Al_xGa_{1-x}N$ bandgap variation essentially follows a linear trend for dilute $Al_xGa_{1-x}N$, where $x \leq 0.063$ and the bowing parameter (b) extracted from formula 1 is equal to 0.9 eV which is close to widely accepted value, b = 1 eV. Additionally, the activation energies of electron emission (E_A) from the two deep-level defects observed in $Al_xGa_{1-x}N$ layers, E1 and E3, also depend linearly on Al content, since higher Al concentration results in corresponding changes in the lattice constant of $A_xlGa_{1-x}N$ alloys.

(2) In turn, the conventional DLTS results shown in this paper suggest that the E3 traps concentration measured in the sub-surface region of the $Al_{0.05}Ga_{0.95}N$ sample (0.3–0.7 μm from the surface), significantly varies along the sample. E3 trap concentrations are much higher closer to the edge than that in sample center. This result is consistent with the PL observation of Fe_{Ga}^{3+} charge state photoluminescence intensity shown in Fig. 8. The SIMS results shown in Fig. 2 confirm that the concentration of residual Fe near the wafer edge is significantly higher than that in the wafer center. This conclusion is consistent with the results reported for Fe_{Ga} in GaN.[12] It should be noted that according to previous reports, the intensity of Fe^{3+}-related luminescence is independent of Fe concentration.[23] The intensity of PL due to internal transitions from dopants can be easily saturated, especially if the lifetime of a state is sufficiently long. In this case, it is known that this transition is spin forbidden and its lifetime is in the range of a few ms. In order to avoid the problem of signal saturation, the laser was defocused to a spot approximately 0.5 mm^2. At the same time, very low power was used ($\sim 10\,\mu$W) and under these conditions, a strong correlation between intensity and measured Fe signal has been found. Commonly, the Pl intensities associated with specific defects in n-type semiconductors at low excitation intensities and low temperatures are proportional to the defect concentration.[33] Here, we expect the PL intensity to be proportional to the concentration of $Fe_{Ga}(0/-)$ defects and suggest that PL intensity measurements as a function of excitation can be used and proper excitation energy could be selected for non-saturated PL signal analysis. Therefore, for precise evaluation of low Fe concentration ($\leq 10^{17}\,cm^{-3}$) in dilute $Al_xGa_{1-x}N$ layers, we propose to use PL system working under low power excitation condition. Furthermore, this PL result has been corroborated by the highly consistent findings from our DLTS and SIMS data confirming Fe variations across the wafer.

(3) Despite the significant dependence of the E3 trap concentration varying with the sample position, the E1 trap concentration remains nearly unchanged as observed in Fig. 6. We reasonably infer that the higher series resistance (Rs) observed in SBDs near the sample edge (Fig. 3) is mostly due to relatively high E3 trap concentration in $Al_xGa_{1-x}N$ samples as confirmed by DLTS results as well as by SIMS data. In turn, this suggests that the introduction of higher concentrations of Fe-related defects would result in the degradation of device characteristics and carrier lifetime.

V. CONCLUSIONS

In conclusion, conventional deep-level transient spectroscopy, photoluminescence, and SIMS techniques have been used to characterize deep-level traps in dilute $Al_xGa_{1-x}N$ ($x \leq 0.063$) epilayers grown by MOVPE on highly conductive ammono-GaN substrates. DLTS has been applied to Ni/Au Schottky barrier diodes to determine the properties of electron traps and their activation energies. It was found that both found traps, labeled as E1 and E3, exhibit linear variations of electron-emission rates with Al content for dilute $Al_xGa_{1-x}N$ ($x \leq 0.063$) Furthermore, we analyzed the effect of the E3 electron trap concentration that strongly depends on the position from the edge to the center of the sample wafer. We suggest that the E3 trap level in dilute $Al_xGa_{1-x}N$ is related to the Fe_{Ga} acceptor level, a conclusion that is consistent with the results of Horita *et al.* in GaN.[12] Finally, we infer that the presence of associated defects caused by higher Fe concentrations may lead to the degradation of device characteristics in dilute $Al_xGa_{1-x}N$.

AUTHOR DECLARATIONS

Conflict of Interest

The authors have no conflicts to disclose.

Author Contributions

L. Sun: Conceptualization (lead); Data curation (equal); Visualization (equal); Writing – original draft (lead); Writing – review & editing (equal). **P. Kruszewski:** Conceptualization (equal); Data curation (equal); Supervision (equal); Visualization (equal); Writing – review & editing (equal). **V. P. Markevich:** Conceptualization (supporting); Visualization (supporting); Writing – review & editing (supporting). **C. A. Dawe:** Visualization (supporting); Writing – review & editing (supporting). **A. R. Peaker:** Conceptualization (supporting); Supervision (supporting); Visualization (supporting); Writing – review & editing (supporting). **I. F. Crowe:** Writing – review & editing (supporting). **J. Plesiewicz:** Data curation (supporting); Writing – review & editing (supporting). **P. Prystawko:** Data curation (supporting); Resources (lead); Writing – review & editing (supporting). **Sz. Grzanka:** Data curation (supporting); Writing – review & editing (supporting). **E. Grzanka:** Data curation (supporting); Writing – review & editing (supporting). **R. Jakiela:** Data curation (supporting); Writing – review & editing (supporting). **D. Binks:** Conceptualization (supporting); Writing – review & editing (supporting). **M. P. Halsall:** Conceptualization (supporting); Funding acquisition (lead);

11 May 2024 05:34:50

Supervision (lead); Validation (lead); Visualization (supporting); Writing – review & editing (supporting).

DATA AVAILABILITY

The data that support the findings of this study are available from the corresponding author upon reasonable request.

REFERENCES

[1]Y. Zhang, Z. Chen, W. Li, H. Lee, M. R. Karim, A. R. Arehart, S. A. Ringel, S. Rajan, and H. Zhao, "Probing unintentional Fe impurity incorporation in MOCVD homoepitaxy GaN: Toward GaN vertical power devices," J. Appl. Phys. **127**(21), 215707 (2020).

[2]M. Meneghini, C. De Santi, I. Abid, M. Buffolo, M. Cioni, R. A. Khadar, L. Nela, N. Zagni, A. Chini, F. Medjdoub, G. Meneghesso, G. Verzellesi, E. Zanoni, and E. Matioli, "GaN-based power devices: Physics, reliability, and perspectives," J. Appl. Phys. **130**(18), 181101 (2021).

[3]J. L. Lyons, D. Wickramaratne, and C. G. Van De Walle, "A first-principles understanding of point defects and impurities in GaN," J. Appl. Phys. **129**(11), 111101 (2021).

[4]F. Scrimizzi, F. Cammarata, G. D'Agata, G. Nicolosi, S. Musumeci, and S. A. Rizzo, "The GaN breakthrough for sustainable and cost-effective mobility electrification and digitalization," Electronics **12**(6), 1436 (2023).

[5]S. Pimputkar, J. S. Speck, S. P. DenBaars, and S. Nakamura, "Prospects for LED lighting," Nat. Photonics **3** 180 (2009).

[6]U. K. Mishra, S. Likun, T. E. Kazior, and Y.-F. Wu, "GaN-based RF power devices and amplifiers," Proc. IEEE **96**(2), 287–305 (2008).

[7]A. Alkauskas, M. D. McCluskey, and C. G. Van De Walle, "Tutorial: Defects in semiconductors—Combining experiment and theory," J. Appl. Phys. **119**(18), 181101 (2016).

[8]P. B. Klein, S. C. Binari, K. Ikossi, A. E. Wickenden, D. D. Koleske, and R. L. Henry, "Current collapse and the role of carbon in AlGaN/GaN high electron mobility transistors grown by metalorganic vapor-phase epitaxy," Appl. Phys. Lett. **79**(21), 3527–3529 (2001).

[9]S. Heikman, S. Keller, S. P. DenBaars, and U. K. Mishra, "Growth of Fe doped semi-insulating GaN by metalorganic chemical vapor deposition," Appl. Phys. Lett. **81**(3), 439–441 (2002).

[10]S. Heikman, S. Keller, T. Mates, S. P. DenBaars, and U. K. Mishra, "Growth and characteristics of Fe-doped GaN," J. Cryst. Growth **248**, 513–517 (2003).

[11]C. Freysoldt, B. Grabowski, T. Hickel, J. Neugebauer, G. Kresse, A. Janotti, and C. G. Van De Walle, "First-principles calculations for point defects in solids," Rev: Mod. Phys. **86**(1), 253–305 (2014).

[12]M. Horita, T. Narita, T. Kachi, and J. Suda, "Identification of origin of E_C −0.6 eV electron trap level by correlation with iron concentration in n-type GaN grown on GaN freestanding substrate by metalorganic vapor phase epitaxy," Appl. Phys. Express **13**(7), 071007 (2020).

[13]R. P. Vaudo, X. Xu, A. Salant, J. Malcarne, and G. R. Brandes, "Characteristics of semi-insulating, Fe-doped GaN substrates," Phys. Status Solidi A **200**(1), 18–21 (2003).

[14]S. Leone, F. Benkhelifa, L. Kirste, C. Manz, S. Mueller, R. Quay, and T. Stadelmann, "Suppression of iron memory effect in GaN epitaxial layers," Phys. Status Solidi B **255**(5), 1700377 (2018).

[15]D. Wickramaratne, J.-X. Shen, C. E. Dreyer, A. Alkauskas, and C. G. Van De Walle, "Electrical and optical properties of iron in GaN, AlN, and InN," Phys. Rev. B **99**(20), 205202 (2019).

[16]V. P. Markevich, M. P. Halsall, L. Sun, I. F. Crowe, A. R. Peaker, P. Kruszewski, J. Plesiewicz, P. Prystawko, S. Bulka, and R. Jakiela, "Electric-field enhancement of electron emission rates for deep-level traps in n-type GaN," Phys. Status Solidi B **260**(8), 2200545 (2023).

[17]J. Plesiewicz, P. Kruszewski, V. P. Markevich, P. Prystawko, S. Bulka, M. Hallsal, I. Crowe, L. Sun, and A. R. Peaker, "Deep-level traps in as-grown and electron-irradiated homo-epitaxial n-GaN layers grown by MOVPE," Microelectron. Eng. **274**, 111977 (2023).

[18]P. Kruszewski, V. P. Markevich, A. R. Peaker, J. Plesiewicz, P. Prystawko, M. P. Halsall, and L. Sun, "Alloy splitting of the FeGa acceptor level in dilute AlxGa1−xN," Appl. Phys. Lett. **123**(22), 222105 (2023).

[19]J. Baur, K. Maier, M. Kunzer, U. Kaufmann, and J. Schneider, "Determination of the GaN/AlN band offset via the (-/0) acceptor level of iron," Appl. Phys. Lett. **65**(17), 2211–2213 (1994).

[20]R. Heitz, P. Maxim, L. Eckey, P. Thurian, A. Hoffmann, I. Broser, K. Pressel, and B. K. Meyer, "Excited states of Fe^{3+} in GaN," Phys. Rev. B **55**(7), 4382–4387 (1997).

[21]J. Baur, K. Maier, M. Kunzer, U. Kaufmann, J. Schneider, H. Amano, I. Akasaki, T. Detchprohm, and K. Hiramatsu, "Infrared luminescence of residual iron deep level acceptors in gallium nitride (GaN) epitaxial layers," Appl. Phys. Lett. **64**(7), 857–859 (1994).

[22]J. Baur, M. Kunzer, K. Maier, U. Kaufmann, and J. Schneider, "Determination of the GaN/AIN band discontinuities via the (-/0) acceptor level of iron," Mater. Sci. Eng. B **29**, 61 (1995).

[23]E. Malguth, A. Hoffmann, W. Gehlhoff, O. Gelhausen, M. R. Phillips, and X. Xu, "Structural and electronic properties of Fe^{3+} and Fe^{2+} centers in GaN from optical and EPR experiments," Phys. Rev. B **74**(16), 165202 (2006).

[24]E. Malguth, A. Hoffmann, and M. R. Phillips, "Fe in III–V and II–VI semiconductors," Phys. Status Solidi B **245**(3), 455–480 (2008).

[25]D. Wickramaratne, J.-X. Shen, C. E. Dreyer, M. Engel, M. Marsman, G. Kresse, S. Marcinkevičius, A. Alkauskas, and C. G. Van De Walle, "Iron as a source of efficient Shockley-Read-Hall recombination in GaN," Appl. Phys. Lett. **109**(16), 162107 (2016).

[26]P. Kruszewski, P. Prystawko, M. Grabowski, T. Sochacki, A. Sidor, M. Bockowski, J. Jasinski, L. Lukasiak, R. Kisiel, and M. Leszczynski, "Electrical properties of vertical GaN Schottky diodes on ammono-GaN substrate," Mater. Sci. Semicond. Process. **96**, 132–136 (2019).

[27]M. Zajac, R. Kucharski, K. Grabianska, A. Gwardys-Bak, A. Puchalski, D. Wasik, E. Litwin-Staszewska, R. Piotrzkowski, J. Z. Domagala, and M. Bockowski, "Basic ammonothermal growth of gallium nitride—State of the art, challenges, perspectives," Prog. Cryst. Growth Charact. Mater. **64**(3), 63–74 (2018).

[28]T. Tanaka, K. Shiojima, T. Mishima, and Y. Tokuda, "Deep-level transient spectroscopy of low-free-carrier-concentration n-GaN layers grown on freestanding GaN substrates: Dependence on carbon compensation ratio," Jpn. J. Appl. Phys. **55**(6), 061101 (2016).

[29]Y. Tokuda, "(Invited) DLTS studies of defects in n-GaN," ECS Trans. **75**(4), 39–49 (2016).

[30]A. R. Peaker, V. P. Markevich, and J. Coutinho, "Tutorial: Junction spectroscopy techniques and deep-level defects in semiconductors," J. Appl. Phys. **123**(16), 161559 (2018).

[31]D. Stievenard and D. Vuillaume, "Profiling of defects using deep level transient spectroscopy," J. Appl. Phys. **60**(3), 973–979 (1986).

[32]N. Nepal, M. L. Nakarmi, J. Y. Lin, and H. X. Jiang, "Photoluminescence studies of impurity transitions in AlGaN alloys," Appl. Phys. Lett. **89**(9), 092107 (2006).

[33]M. A. Reshchikov, "Photoluminescence from defects in GaN," in *Gallium Nitride Materials and Devices XVIII*, edited by H. Morkoç, H. Fujioka, and U. T. Schwarz (SPIE, San Francisco, 2023), p. 17.